On the existence of piezo-electrogyration in crystals

2000 J. Phys.: Condens. Matter 12 1485

(http://iopscience.iop.org/0953-8984/12/7/329)

J. Phys.: Condens. Matter **12** (2000) 1485–1496. Printed in the UK PII: S0953-8984(00)04910-9

On the existence of piezo-electrogyration in crystals

H-J Weber†, E V Balashova‡ and S A Kizhaev‡

† Institut für Physik, Universität Dortmund, D-44221 Dortmund, Germany
‡ A F Ioffe Physical Technical Institute, St Petersburg 194021, Russia

E-mail: weberhj@fkp.physik.uni-dortmund.de

Received 2 June 1999, in final form 10 November 1999

Abstract. It is shown that crystals with the symmetry $m3$ and $m3m$ are suitable materials to study if one is seeking to detect the dependence of electrogyration on stress which is described by an axial tensor of rank five. Experiments are performed on methylammonium alums doped with chromium. Several properties of the material enable critical checks of experimental results to be made. The checks are needed because the intrinsic effect is usually smaller than effects which are caused by the interaction of linear and circular optical properties but which are no signature of intrinsic piezo-electrogyration. At room temperature a stress-induced electrogyration of 6×10^{-17} V^{-1} Pa^{-1} has been observed. At a temperature of 200 K which is 25 K above the transition into the ferroelectric phase the magnitude of the stress-induced circular electrodichroism is 10^{-15} V^{-1} Pa^{-1} in a sample with 10% chromium. These magnitudes are considered to represent upper limits of piezo-electrogyration in crystals because they result from special properties of the doped alum.

1. Introduction

The generation of optical activity or gyration by the simultaneous action of elastic and electric fields is investigated for the first time. We call this effect piezo-electrogyration. Due to the high sensitivity of polarization–optical experiments the effect has the potential to provide a tool for studying the coupling of electric and elastic fields in centrosymmetric solids. The two underlying effects, electrogyration [1–7] and piezogyration [8–11], have already been studied in the past. From these investigations it is well known that the determination of intrinsic gyration effects can be impeded by the influence of various disturbing effects which are sometimes difficult to control [2, 9, 11]. Electric-field-induced changes of the polarization state of light are modified by stress-induced linear birefringence. This interaction simulates the existence of piezo-electrogyration and is called false piezo-electrogyration in the following. Due to its crucial influence on the measurements it is important to optimize the conditions of an experimental performance and to select a material that is most suitable for investigation as regards the detection of piezo-electrogyration. Our intention is to show solutions of experimental problems, to demonstrate the existence of an intrinsic effect, and to determine its order of magnitude.

Gyration or optical activity manifests itself as circular birefringence ρ or as circular dichroism σ which are related to the scalar parameter of gyration $g = g' + \mathrm{i}g''$ by [12]

$$\rho L = \frac{\pi L}{\lambda n} g' \qquad \text{and} \qquad \sigma L = \frac{\pi L}{\lambda n} g''.$$

0953-8984/00/071485+12$30.00

Here L is the thickness of the sample, n is the index of refraction, and λ is the wavelength of light. For transparent materials, $g'' = \sigma = 0$. If linear birefringence

$$\delta L = \frac{\pi}{\lambda} \Delta n \, L$$

is absent, ρ describes the specific rotation and σ the specific ellipticity imposed on a linearly polarized light wave.

In section 2 we discuss some properties which a crystal should possess for it to be considered a suitable material to select for studying piezo-electrogyration. Experimental details are described in section 3 and results are presented in section 4. The dispersion of electric-field-induced circular birefringence and dichroism (subsection 4.1) tells us that induced circular optical effects of the Cr^{3+} resonance can be determined by measurements at *one* wavelength. This reduces the number of measurements in the stress experiments to an acceptable level even in the study of phase transitions. The influence of false piezo-electrogyration and some features of the intrinsic effect are discussed in subsections 4.2 and 4.3, respectively.

2. Influence of symmetry and linear birefringence

The scalar parameter of gyration depends on the unit wavevector $\boldsymbol{l}$ as $g = g_{ij} l_i l_j$, where g_{ij} represents an axial tensor of rank two. Several arguments suggest studying the dependence of g on electric field $\boldsymbol{E}$ and on uniaxial stress $\boldsymbol{T}$ in cubic crystals with a centre of symmetry:

(i) There is no large linear birefringence which quenches gyration effects.
(ii) The disturbing influence of the linear electro-optical effect is absent.
(iii) It can be shown that piezo-electrogyration is absent in isotropic materials such as glasses which otherwise would be more suitable than crystals.
(iv) Crystals of the non-centrosymmetric point symmetry group (PSG) 432 also fulfil requirements (i) and (ii). However, they also show the disturbing property of a linear electro-optical effect induced by uniaxial stress.
(v) In contrast to the case for non-cubic crystals, requirement (i) does not restrict the propagation of light waves in cubic samples. Different propagation directions are needed if the anisotropy of the effect is to be studied.

Non-cubic crystals can be used with profit if one wants to study the influence of linear birefringence for a large range of δL. The value of δL for a light wave which propagates approximately along the optical axis can be adjusted by a small rotation of the sample. We did not carry out this experiment because it needs a special device to align the specimen under stress precisely and because of the advantages related to the use of cubic crystals. Thus, we are left with the two cubic point symmetry groups $m3$ and $m3m$. Expanding the gyration tensor in terms of $\boldsymbol{E}$ and $\boldsymbol{T}$ we obtain for crystals with a centre of symmetry

$$g_{ij} = s_{ijk} E_k + t_{ijklm} E_k T_{lm}. \tag{1}$$

All coefficients in equation (1) are complex for absorbing crystals and they are components of axial tensors. The identities $g_{ij} = g_{ji}$ and $T_{ij} = T_{ji}$ reduce the number of independent coefficients. Further reduction is obtained by the action of symmetry operations. In the PSG $m3$ one independent electrogyration coefficient exists: $s_{123} = s_{231} = s_{312}$ [1]. The effect is absent in the PSG $m3m$ and in isotropic materials. Using the direct inspection method we have evaluated the tensor components of the coupling effect t_{ijklm}. The results for the PSGs $m3$ and $m3m$ are presented in table 1. The large number of independent components in PSG $m3$ renders the determination of the tensor difficult and prevents a consistency check

Table 1. Components of the piezo-electrogyration tensor in PSG $m3$ and PSG $m3m$.

PSG	No	t_{ijklm}
$m3$	1	$t_{11123} = t_{22213} = t_{33312}$
	2	$t_{11213} = t_{22312} = t_{33123}$
	3	$t_{11312} = t_{22123} = t_{33213}$
	4	$t_{12113} = t_{23212} = t_{13323}$
	5	$t_{13112} = t_{12223} = t_{23313}$
	6	$t_{12311} = t_{23122} = t_{13233}$
	7	$t_{13211} = t_{12322} = t_{23133}$
	8	$t_{23111} = t_{13222} = t_{12333}$
$m3m$	1	$t_{11213} = t_{22312} = t_{33123} = -t_{11312} = -t_{22123} = -t_{33213}$
	2	$t_{12113} = t_{23212} = t_{13323} = -t_{13112} = -t_{12223} = -t_{23313}$
	3	$t_{12311} = t_{23122} = t_{13233} = -t_{13211} = -t_{12322} = -t_{23133}$

of the observed results by performing measurements with different directions of $\boldsymbol{E}$, $\boldsymbol{T}$, and wavevector $\boldsymbol{k}$.

To avoid inhomogeneous stresses the sample should be sufficiently thick. This in turn requires small absorption of light because otherwise transmission experiments are impossible. Reflection experiments are useless because ρ and σ are reciprocal circular properties. A suitable material seems to be one with a wide band-gap and which is doped with transition metal ions. In such a material the stress-induced linear dichroism κ is significantly smaller than the stress-induced birefringence δ. If, in addition, the linear birefringence is much larger than the circular birefringence and circular dichroism, the influence of the sample on the polarization state of a transverse wave is given by the Jones matrix

$$\begin{pmatrix} \cos\delta L - \mathrm{i}\sin\delta L & -\rho L\dfrac{\sin\delta L}{\delta L} - \mathrm{i}\sigma L\dfrac{\sin\delta L}{\delta L} \\ \rho L\dfrac{\sin\delta L}{\delta L} + \mathrm{i}\sigma L\dfrac{\sin\delta L}{\delta L} & \cos\delta L + \mathrm{i}\sin\delta L \end{pmatrix}. \tag{2}$$

Here we have assumed that the x- and y-axes of the reference system are parallel to the axes of δ. The conditions $\delta \gg \kappa, \rho, \sigma$ are useful because otherwise the transfer matrix (2) gets more complicated. On the other hand the factor $(\sin\delta L)/\delta L$ should not be significantly smaller than *one*. Crystals which fulfil these conditions include alums doped with chromium which crystallize in the cubic point symmetry group $m3$. In these crystals the octahedral {111} faces are morphologically dominant. Perpendicular to each trigonal [111] axis the doped crystals are birefringent. Thus, one single crystal contains eight growth sectors [3]. The concentration of chromium can be chosen in such a way that the conditions $\delta \gg \rho, \sigma$ are fulfilled without quenching the circular effects and that δ induced by doping is bigger than δ induced by stress which reduces the misleading influence of inhomogeneous stress components. We have selected the alum methylammonium-aluminium-sulphate-dodecahydrate $CH_3NH_3Al(SO_4)_2{\cdot}12H_2O$ (abbreviated as MASD). In the doped crystals, Cr^{3+} substitutes for Al^{3+} (abbreviated as M(Al, Cr)SD). MASD has a transition into the ferroelectric phase at $\mathcal{T}_C = 176.4$ K [14]. We have measured the dielectric constant and the speed of longitudinal elastic waves in a sample doped with 11.2 mol% Cr^{3+}. The results are shown in figure 1. They demonstrate the softening of the dielectric susceptibility and of the elastic constants just above the transition temperature $\mathcal{T}_C$. As both susceptibilities are involved in the measurement of piezo-electrogyration, the effect should increase near $\mathcal{T}_C$. Furthermore, the dependence of $\partial^2\sigma/(\partial E\,\partial T)$ on the chromium content may serve as a reliability check. In conclusion, M(Al, Cr)SD seems to be an ideal material for use in deciding whether piezo-electrogyration is observable in crystals or not.

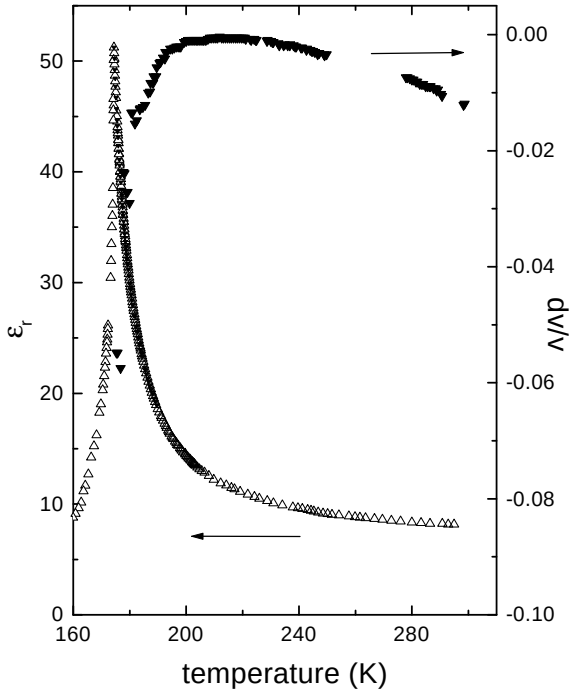

Figure 1. The relative dielectric constant ϵ_r as a function of temperature and relative changes of the velocity v of a longitudinal ultrasonic wave propagating along [100] in M(Al, Cr)SD.

3. Experimental procedure

3.1. Samples

Single crystals of M(Al, Cr)SD were grown by the slow evaporation of aqueous solutions. We have studied mainly four rectangular samples cut out of one growth section. The dimensions, chromium concentrations, and linear birefringences due to doping are given in table 2. Samples SI and SIII were used for dispersion measurements and samples SII, SIII, and SIV were used for stress measurements. Table 2 also shows the orientations of wavevector $\boldsymbol{k}$, electric field $\boldsymbol{E}$, and stress $\boldsymbol{T}$ with respect to the crystallographic axes.

There is no simple reason for the appearance of homogeneous optical birefringence, because Al^{3+} and Cr^{3+} alums form mixed crystals. Nevertheless, this anomalous phenomenon exists and in a strict sense the mixed crystals show a trigonal symmetry with the ordinary index of refraction n_o perpendicular to [111]. In M(Al, Cr)SD, n_o is smaller than n_e. In several cases the influence of different growth sectors prevented the production of homogeneous stress. Measurements on these samples have been removed from the final analysis of the data.

3.2. Experimental set-up

The optical system of the experimental set-up consists of the light source, a polarizer, the sample, a Faraday rotator, an analyser, and the detector which is a photomultiplier [13]. The azimuthal orientations of the polarizer and of the analyser are denoted by the angles ϕ and α, respectively. Both optical components are rotated in steps of 0.01 degrees. In a second configuration a quarter-wave plate is inserted between the sample and the Faraday rotator. The Faraday rotator is driven by an alternating current at the frequency $\nu_{FR} \approx 700$ Hz and the frequency of the electric field is $\nu \approx 200$ Hz. Both intensity signals, $I(\nu_{FR})$ and $I(\nu)$, are

Table 2. Dimensions L (unit: mm), chromium content, and linear birefringence δL (unit: degrees) of samples; orientations of the wavevector $\boldsymbol{k}$, electric field $\boldsymbol{E}$, and stress $\boldsymbol{T}$; together with effective tensor constants s_{ijk} and t_{ijklm}.

	SI	SII	SIII	SIV
$\boldsymbol{L} \parallel [1\bar{1}0]$	7.14	5.26	3.11	2.49
$\boldsymbol{L} \parallel [11\bar{2}]$	12.34	10.18	4.58	8.82
$\boldsymbol{L} \parallel [111]$	9.80	19.68	6.50	4.96
mol% Cr^{3+}	4.8	5.6	11.2	11.2
δL	39.4	42.0	29.7	32.1
$\boldsymbol{k}$	$[1\bar{1}0]$	$[1\bar{1}0]$	$[1\bar{1}0]$	$[11\bar{2}]$
$\boldsymbol{E}$	[111]	[111]	[111]	$[1\bar{1}0]$
$\boldsymbol{T}$	—	$[11\bar{2}]$	[111]	$[1\bar{1}0]$
s_{ijk}	s^*	s^*	s^*	0
t_{ijklm}	—	t^*	t^{**}	t^{***}

$s^* = -s_{123}/\sqrt{3}$

$t^* = \frac{\sqrt{3}}{9}[2(t_{11123} + t_{11213} + t_{11312} - t_{12113} - t_{12223}) - t_{12311} - t_{12322} - t_{12333}]$

$t^{**} = \frac{-\sqrt{3}}{18}[4(t_{11123} - t_{12113} - t_{12223} + t_{12333}) + t_{11213} + t_{11312} + t_{12311} + t_{12322}]$

$t^{***} = \frac{\sqrt{2}}{3}[t_{21223} - t_{12113}] + \frac{\sqrt{2}}{6}[t_{21322} - t_{12311}]$

recorded by lock-ins. Dispersion measurements are performed with a continuous light source. The dependences of $\partial\rho/\partial E$ and $\partial\sigma/\partial E$ on stress are determined at $\lambda = 633$ nm by use of a He–Ne laser. The sample holder in the cryostat is provided with a spring which produces stress up to about 1 MPa. At room temperature, higher stresses have been achieved by loading the sample with weights.

3.3. Recorded signals

At first we search for the azimuthal orientation of the polarizer and the analyser at which the transmitted intensity shows a minimum. At these positions the direction of polarization coincides approximately with the principal axis of birefringence ($\phi \approx 0$) and the analyser is oriented perpendicularly to the polarizer ($\alpha \approx 0$). In addition, the configuration $\phi \approx 90$ degrees together with $\alpha \approx 90$ degrees is used.

The polarization state of the light wave leaving the sample is described by the azimuthal orientation θ and the ellipticity ϵ. In all measurements, the residual ellipticities stemming from a small misorientation of the polarizer are negligibly small. At first we consider the configuration without the quarter-wave plate. The orientation of the analyser α is changed in steps of 0.01 degrees in order to obtain the accurate position at which the signals vanish and to determine the slopes:

$$\frac{\partial I(\nu)}{\partial \alpha} = -2\theta(\nu) I_0 \qquad \text{and} \qquad \frac{\partial I(\nu_{FR})}{\partial \alpha} = -2\rho_{FR} I_0 \tag{3}$$

where ρ_{FR} denotes the effect of the Faraday rotator. Rotating the polarizer instead of the analyser we obtain

$$\begin{aligned} \frac{\partial I(\nu)}{\partial \phi} &= -2[\cos(2\delta L)\theta(\nu) \pm \sin(2\delta L)\epsilon(\nu)] I_0 \\ \frac{\partial I(\nu_{FR})}{\partial \phi} &= 2\cos(2\delta L)\rho_{FR} I_0 \end{aligned} \tag{4}$$

where the upper and the lower sign are valid for $\phi = 0$ and $\phi = 90$ degrees, respectively. After the quarter-wave plate is inserted, its azimuthal orientation and that of the analyser are adjusted in such a way that the transmitted intensity is minimal and $I(\nu_{FR}) = 0$. Starting with this position of the analyser, a small rotation yields

$$\frac{\partial I(\nu)}{\partial \alpha} = 2\epsilon(\nu) I_0 \qquad \text{and} \qquad \frac{\partial I(\nu_{FR})}{\partial \alpha} = -2\rho_{FR} I_0. \tag{5}$$

In equations (3)–(5) I_0 is assumed to be the incoming intensity containing all losses due to reflection and absorption. The signal $\partial I(\nu_{FR})/\partial\alpha$ is used to calibrate $I(\nu)$, and $\partial I(\nu_{FR})/\partial\phi$ is used to determine the linear birefringence.

In the case of an homogeneous birefringent sample, $\theta(\nu)$ and $\epsilon(\nu)$ are given by

$$\begin{aligned} \theta(\nu) &= \left[\frac{\sin 2\delta L}{2\delta} \frac{\partial \rho}{\partial E} \mp \frac{\sin^2 \delta L}{\delta} \frac{\partial \sigma}{\partial E} \right] E(\nu) \\ \epsilon(\nu) &= \left[\pm \frac{\sin^2 \delta L}{\delta} \frac{\partial \rho}{\partial E} + \frac{\sin 2\delta L}{2\delta} \frac{\partial \sigma}{\partial E} \right] E(\nu). \end{aligned} \tag{6}$$

Inserting equation (6) into the expressions for $\partial I(\nu)/\partial\alpha$ (equations (3) and (5)) and into the expression for $\partial I(\nu)/\partial\phi$ (equation (4)), the terms containing induced gyration $\partial\rho/\partial E$ and induced circular dichroism $\partial\sigma/\partial E$ are separated by adding and subtracting the signals observed for $\phi = 0$ (upper signs) and $\phi = 90$ degrees (lower sign).

4. Results

4.1. Dispersion of electrogyration

Cr^{3+} ions show two broad absorption bands in the visible range of the optical spectrum. In M(Al, Cr)SD they are centred at 409 nm and at 572 nm, respectively. Typical resonance phenomena are observed for $\partial\rho/\partial E$ and $\partial\sigma/\partial E$ near the 572 nm absorption band [3]. Using the Rosenberg–Condon [15] dispersion formula the contribution of this band is given by

$$\left(\frac{\partial \sigma}{\partial E}\right)_{\mathrm{Cr}} = \frac{B\lambda}{(\lambda^2 - \lambda_0^2)^2 + C\lambda^2} \tag{7}$$

and

$$\left(\frac{\partial \rho}{\partial E}\right)_{\mathrm{Cr}} = \frac{B}{\sqrt{C}} \frac{\lambda^2 - \lambda_0^2}{(\lambda^2 - \lambda_0^2)^2 + C\lambda^2}. \tag{8}$$

In equations (7) and (8) λ_0 is the resonance wavelength, C is a damping constant, and B is a measure of the oscillator strength. Two types of formula are known which describe the dispersion of rotatory power [16]. For $\lambda \ll \lambda_0$ the second term in the denominator of equation (8) is small and the wavelength dependence reduces to $\partial\rho/\partial E \propto 1/(\lambda^2 - \lambda_0^2)$ which is identical to Drude's formula for $\rho(\lambda)$. For all transparent alums, the electric-field-induced rotatory power is well described by the second type of dispersion which represents a model for compound oscillators [4]. Assuming that this type of dispersion is also valid for the contribution $(\partial\rho/\partial E)_0$ of the optical transitions at high photon energies in the doped alum, the total field-induced rotatory power is given by

$$\frac{\partial \rho}{\partial E} = \left(\frac{\partial \rho}{\partial E}\right)_0 + \left(\frac{\partial \rho}{\partial E}\right)_{\mathrm{Cr}} = A \frac{\lambda^2}{(\lambda^2 - 88^2)^2} + \left(\frac{\partial \rho}{\partial E}\right)_{\mathrm{Cr}}. \tag{9}$$

We have determined the dispersion of $\partial\rho/\partial E$ and $\partial\sigma/\partial E$ in two samples with chromium concentrations of 4.8 (sample SI) and 11.2 (sample SIII) mol%. Birefringences range from

$\delta_{min} = 27.0$ degrees (sample SIII, $\lambda = 700$ nm) to $\delta_{max} = 65.0$ degrees (sample SI, $\lambda = 425$ nm). Results obtained at room temperature are presented in figure 2. Obviously, the magnitude of A decreases and the magnitude of B increases with increasing chromium concentration. At room temperature these relationships are approximately linear. With decreasing temperature $|B/A|$ becomes smaller which is consistent with previous results [17]. Within the experimental accuracy we find no variation of the resonance wavelength λ_0 and of the damping constant C as a function of temperature or chromium concentration. The average results are $\lambda_0 = 602.7$ nm and $C = 6920$ nm^2.

4.2. Stress-induced effects

As the structural changes induced by variations of temperature and doping have no influence on the parameters λ_0 and C, it is reasonable to assume that these parameters are also independent of stress. Equations (7)–(9) show that in this case the measurement of $\partial\rho/\partial E$ and $\partial\sigma/\partial E$ at *one* wavelength enables the determination of the two dispersion parameters A and B. A suitable wavelength is $\lambda = 633$ nm for the He–Ne laser which we use to determine piezo-electrogyration. Table 2 shows the orientations of $\boldsymbol{k}$, $\boldsymbol{E}$, and $\boldsymbol{T}$ used and the combinations of tensor components which are observed with these configurations. A comparison of the data in table 1 and table 2 shows that the chosen stress configurations for samples SII and SIII probe all independent tensor components and thereby all mechanisms which may contribute to the piezo-electrogyration effect.

To illustrate the interactions between the electric-field-induced circular effects and the linear birefringence, we consider the measurements with $\boldsymbol{T} \parallel [11\bar{2}]$ performed on sample SII. Two types of expression are extracted from the set of six measurements described by equations (3)–(5). They read

$$S_\alpha = \frac{\sin 2\delta L}{2\delta} K_\alpha \qquad \text{and} \qquad S_\beta = \frac{\sin^2 \delta L}{\delta} K_\beta \tag{10}$$

where K_α and K_β represent $\partial\rho/\partial E$ or/and $\partial\sigma/\partial E$. We present the observed birefringences in figure 3, and examples for S_α and S_β with $K_\alpha = K_\beta = \partial\rho/\partial E$ observed at 293 K and at 229 K in figure 4. The data at 229 K have been reduced by a common factor in order to eliminate the temperature dependence of the electrogyration. Figure 4 demonstrates the strong influence of δ on the detectable signals. As this influence is significantly different for S_α and S_β, systematic errors in δL are averaged out by use of both types of quantity, at least to some extent.

Systematic errors stem from inhomogeneous stress and from a special kind of birefringent domain. These domains have the same orientation as but the opposite sign to the main birefringence. As they are small and randomly distributed, the samples seem to be homogeneous. However, in such domains some terms of equations (3)–(6) remain unaffected and some change their signs, which modifies the signals $\partial I(\nu)/\partial\alpha$ and $\partial I(\nu)/\partial\phi$. Measurements performed with inhomogeneous stress were removed from the final analysis of the data. We did not refine the experimental data by an appropriate domain model. Thus, the influence of domains is contained in the error bars shown in figures 5–8.

The results for $\partial\rho/\partial E$ and $\partial\sigma/\partial E$ observed in sample SII are presented in figures 5 and 6. Comparing figure 5 with figure 1 we find that $\partial\rho/\partial E$ increases significantly more strongly than the dielectric constant ϵ_r with decreasing temperature. This behaviour results from the fact that the phase transition is not intrinsically ferroelectric [18]. Figure 5 shows no significant dependence of $\partial\rho/\partial E$ on stress. Such a dependence is demonstrated in figure 6 by $\partial\sigma/\partial E$ observed at 229 K and 204 K. The signs of the slopes of S_α and S_β are the same between 204 K and 293 K (see figures 3 and 4), the piezo-optical effect is the same for 229 K and 204 K (see figure 3), and all experimental conditions were the same at different temperatures. Thus, there

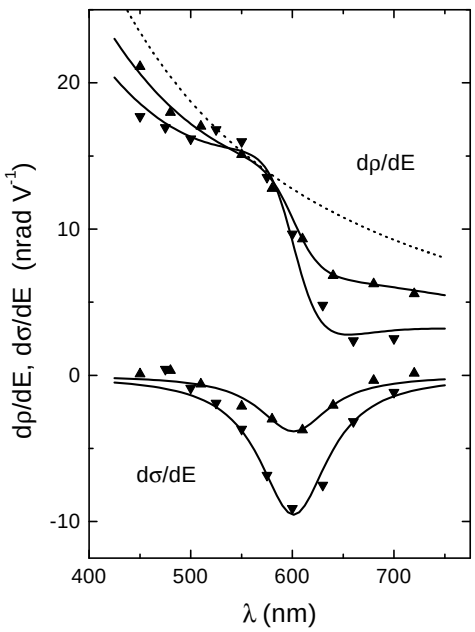

Figure 2. The dispersion of the electric-field-induced circular birefringence $\partial\rho/\partial E$ and circular electrodichroism $\partial\sigma/\partial E$ at room temperature for sample SI (up-pointing triangles) and sample SIII (down-pointing triangles). Solid lines are fits of the dispersion formulae (7)–(9). The dotted line shows the dispersion of the pure alum MASD.

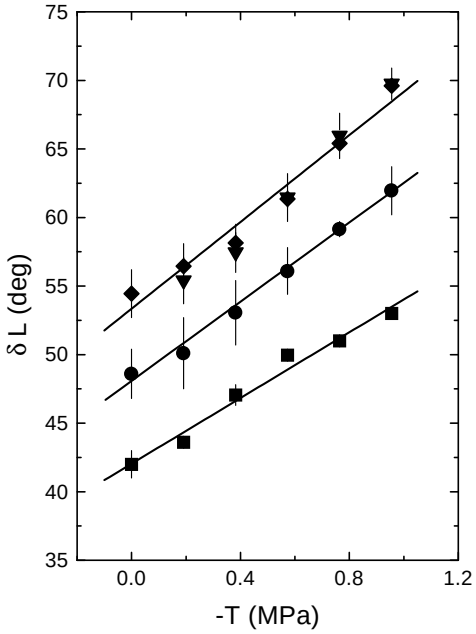

Figure 3. Linear birefringence as a function of uniaxial stress for sample SII. The wavelength is $\lambda = 633$ nm and the temperatures are 293 K (squares), 259 K (circles), 229 K (triangles), and 204 K (diamonds). Lines are least-squares fits which are the same for 229 K and 204 K.

is no way to trace back the finite values of $\partial^2\sigma/(\partial E\,\partial T)$ at 229 K and 204 K to the uncontrolled influence of an unknown error parameter. These results have to be considered as the intrinsic piezo-electrogyration effect.

The stress effect shown in figure 6 is presented in figure 7 as a function of temperature together with the results observed for sample SIII ($\boldsymbol{T} \parallel [111]$). The error parameters are larger for sample SIII than for sample SII because it was possible to optimize the sample dimensions for the configuration $\boldsymbol{E} \parallel [111]$, $\boldsymbol{T} \parallel [11\bar{2}]$ (sample SII) but not for the configuration $\boldsymbol{E} \parallel \boldsymbol{T} \parallel [111]$ (sample SIII). In the latter case the rather small value for the thickness parallel to [111] (see table 2) which is favourable for the creation of large electric-field-induced effects makes the production of a homogeneous stress difficult. The absence of any stress effect for $\boldsymbol{T} \parallel [11\bar{2}]$ above $\mathcal{T}^*$ may happen by accident because the effective tensor constant of this configuration contains a combination of eight different components as shown in table 2. We have checked at room temperature for two additional samples that the stress effect for $\boldsymbol{T} \parallel [111]$ decreases with decreasing chromium content. However, figure 7 illustrates that the relative errors are rather large for temperatures above $\mathcal{T}^*$. To obtain more convincing results at room temperature we have performed measurements with the configuration shown in table 2 for sample SIV. In this case stress-free electrogyration is absent which renders the detection of the intrinsic stress-induced effect more reliable than for the configurations used with samples SII and SIII. In addition the dimensions of sample SIV have been chosen in such a way that a maximum of stress was achievable. Results are presented in figure 8. The stress-induced effects are clearly larger than the experimental errors. In particular the data for

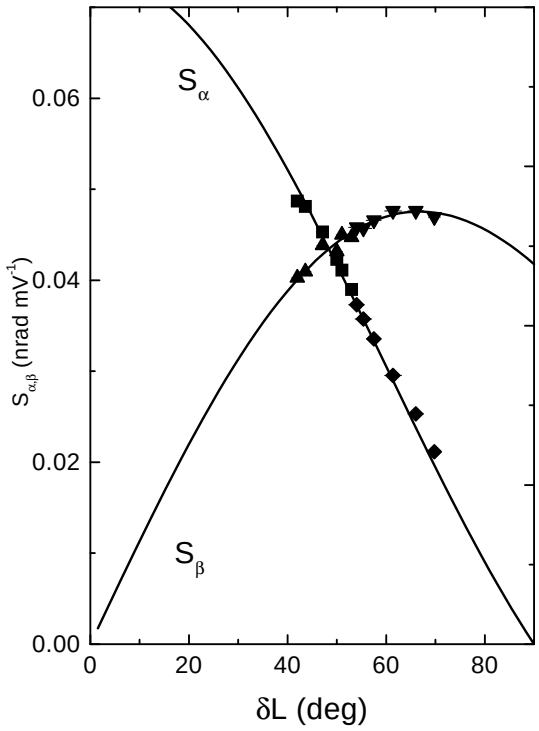

Figure 4. Signals S_α and S_β as defined in equation (11) for $K_\alpha = K_\beta = \partial\rho/\partial E$ as functions of the linear birefringence. Solid lines are best fits. The experimental data are valid for the thickness of sample SII given in table 2. Squares and up-pointing triangles: 293 K; diamonds and down-pointing triangles: 229 K (the data are modified as explained in the text).

$\partial\sigma/\partial E$ demonstrate that the stress is responsible for the non-zero effect. The non-vanishing effect on $\partial\rho/\partial E$ at $T = 0$ does not stem from a misalignment of the sample but should be considered as consequence of the trigonal distortion of the crystal.

4.3. Features of piezo-electrogyration in M(Al, Cr)SD

Figure 7 indicates the existence of two different mechanisms of the stress effect. Above $\mathcal{T}^* \approx 230$ K, $\partial^2\sigma/(\partial E\,\partial T)$ is independent of temperature in sample SIII and absent in sample SII. Below $\mathcal{T}^*$ an additional increase occurs in both samples which is related to the elastic anomaly near the structural phase transition indicated by the change of the slope $\partial \ln v/\partial T$ at $\mathcal{T}^*$ (see figure 1). The increase of $\partial^2\sigma/(\partial E\,\partial T)$ is most probably described by the tensor components t_{123mm} ($m = 1, 2, 3$) since they have the same sign in both stress configurations as shown in table 2. The magnitudes of the piezo-electrogyration effects for $\boldsymbol{E} \parallel \boldsymbol{T} \parallel [1\bar{1}0]$ at room temperature are $\partial^2\rho/(\partial E\,\partial T) = 0.065(7) \times 10^{-15}$ V^{-1} Pa^{-1} and $\partial^2\sigma/(\partial E\,\partial T) = -0.121(9) \times 10^{-15}$ V^{-1} Pa^{-1}. The latter result is about six times smaller than the result for $\boldsymbol{E} \parallel \boldsymbol{T} \parallel [111]$ (see figure 7). The value of $\partial^2\rho/(\partial E\,\partial T)$ observed for sample SIV shows the magnitude of the experimental errors observed at room temperature for sample SII where the stress-free electrogyration effect is not absent.

Using equations (7)–(9) and assuming that the stress changes the dispersion parameters A and B but not λ_0 and C as discussed in the preceding section, we are in a position to determine the piezo-electrogyration effect $(\partial^2\rho/\partial E\,\partial T)_0$ which contains all contributions of optical transitions at high photon energies ($h\nu > 3$ eV). Within the experimental accuracy we find no effect for $\boldsymbol{T} \parallel [11\bar{2}]$ (sample SII). For $\boldsymbol{T} \parallel [111]$ (sample SIII) we observe an increasing effect of the stress with decreasing temperature. As $(\partial\rho/\partial E)_0$ itself increases too,

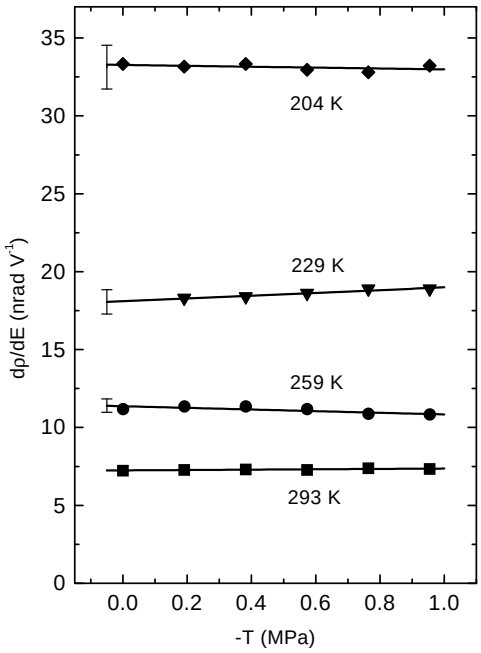

Figure 5. The electric-field-induced circular birefringence of sample SII as a function of uniaxial stress. The symbols are related to the same temperatures as in figure 3.

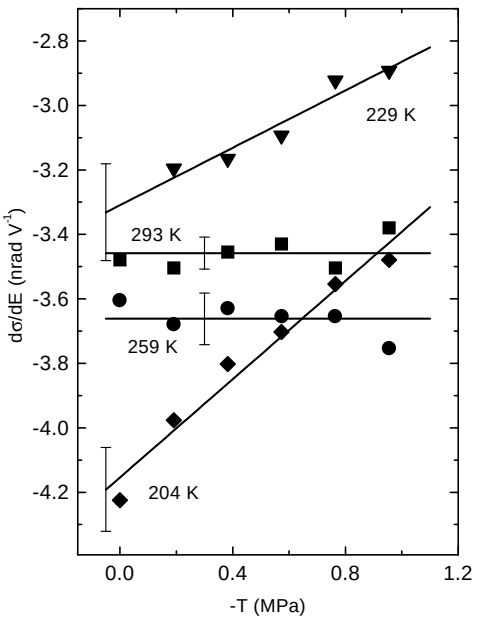

Figure 6. The circular electrodichroism of sample SII. The symbols are the same as in figure 3.

the relative changes are constant. The average value observed in the range of temperatures shown in figure 7 is

$$\frac{\partial \ln(\partial\rho/\partial E)_0}{\partial T} = 0.04 \pm 0.02 \ (\mathrm{MPa}^{-1}). \tag{11}$$

As shown by figures 6 and 7 the relative changes of $\partial\sigma/\partial E$ are even larger (10%–20% per MPa).

Now we compare result (11) with an estimation of the order of magnitude of the effect. For this purpose we consider different stress-induced optical effects. If we assume that a representative value of the natural birefringence in crystals is $\Delta n_{rep} = 0.01$, we calculate from the piezo-optical effect shown in figure 3 relative changes of

$$\frac{\partial\, \Delta n}{\partial T\, \Delta n_{rep}} = 4 \times 10^{-4}\ \mathrm{MPa}^{-1}.$$

The value of

$$\frac{\partial \ln \rho}{\partial T} = 5 \times 10^{-4}\ \mathrm{MPa}^{-1}$$

has been reported for piezogyration in $NaClO_3$ [9]. Equation (11) shows that the piezo-electrogyration in M(Al, Cr)SD is two orders of magnitude larger than suggested by the two estimates. We believe for the following reasons that this difference reflects singular properties of the material under investigation.

(i) The electrogyration effect $\partial\rho/\partial E$ varies by three orders of magnitude in thirty alums among which MASD shows one of the largest effects. $\partial\rho/\partial E$ varies so strongly since

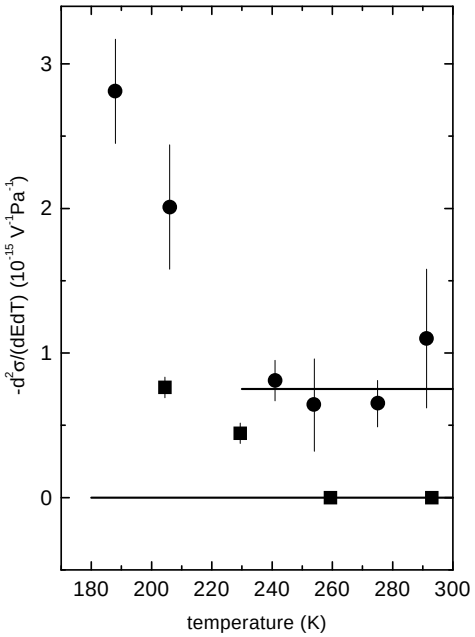

Figure 7. The piezo-electrogyration of sample SII (squares, $\boldsymbol{T} \parallel [11\bar{2}]$) and that of sample SIII (circles, $\boldsymbol{T} \parallel [111]$).

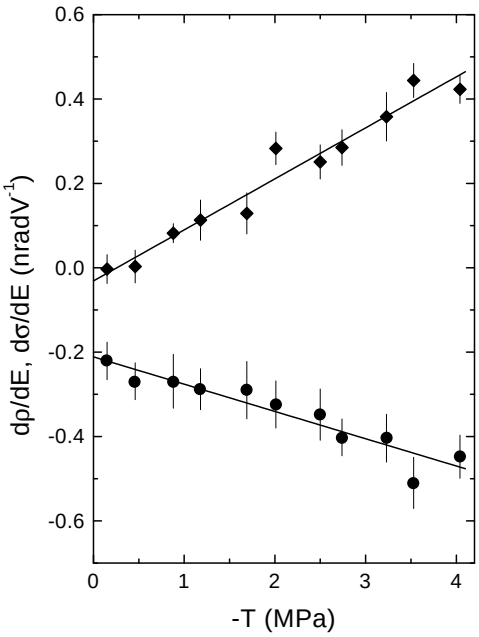

Figure 8. The stress-induced electrogyration (circles) and circular electrodichroism (diamonds) of sample SIV at room temperature.

different structural units of the alums contribute with opposite signs to the total effect. The same should happen for the stress-induced effect.

(ii) The observed effect at low temperatures is obviously related to the structural instabilities which are responsible for the phase transition at $\mathcal{T}$.

(iii) The electric-field-induced effect of the chromium ions is proportional to $\sin\psi$ where the angle ψ denotes the inclination of the surrounding H_2O octahedra relative to the cubic axes [17]. As this angle is very small in M(Al, Cr)SD (-1.7 degrees), the relative changes

$$\partial \ln(\partial\sigma/\partial E)_{\mathrm{Cr}}/\partial\psi = \cot\psi \tag{12}$$

are very large.

Points (i) and (ii) explain why result (11) is two orders of magnitude larger than the estimated value. Point (iii) explains the observation that relative changes of circular electrodichroism are larger than relative changes of $(\partial\rho/\partial E)_0$, which does not contain specific contributions from chromium ions.

5. Conclusions

As demonstrated in figure 4, the influence of stress-induced linear birefringence on the electric-field-induced circular birefringence is usually stronger than intrinsic piezo-electrogyration. The influence of false piezo-electrogyration was controlled by recording signals which contain linear birefringence in different ways. The existence of true piezo-electrogyration has been demonstrated by measurements at different temperatures and by use of a configuration for which cubic symmetry forbids electrogyration. Owing to special properties of M(Al, Cr)SD (proximity to a structural phase transition, several structural units which contribute with

opposite signs to the electrogyration), the effect is rather large. We expect that the relative changes of 10^{-8} to 10^{-7} Pa^{-1} which are observed in this material will prove to represent upper limits of piezo-electrogyration.

Acknowledgment

We gratefully acknowledge financial support by the Deutsche Forschungsgemeinschaft.

References

[1] Zheludev I S 1965 *Sov. Phys.–Crystallogr.* **9** 418
[2] Miller A 1973 *Phys. Rev.* B **8** 5902
[3] Weber H-J and Haussühl S 1974 *Phys. Status Solidi* b **65** 633
[4] Weber H-J and Haussühl S 1976 *Acta Crystallogr.* A **32** 892
[5] Stasyuk I V and Kotsur S S 1985 *Phys. Status Solidi* b **130** 103
[6] Vlokh O G, Klepatch N I and Shopa Y I 1986 *Ferroelectrics* **69** 267
[7] Perekalina Z B, Veremeichik T F, Tynaev A D, Grechushnikov B N and Yakovleva L M 1994 *Crystallogr. Rep.* **39** 488
[8] Myers M B and Vedam K 1967 *J. Opt. Soc. Am.* **57** 1146
[9] Weber H-J 1979 *Acta Crystallogr.* A **35** 225
[10] Babonas G A and Reza A A 1982 *Sov. Phys.–Crystallogr.* **27** 559
[11] Koopmans B, Etchegoin P, Santos P and Cardona M 1996 *Solid State Commun.* **97** 261
[12] Yariv A and Yeh P 1984 *Optical Waves in Crystals* (New York: Wiley)
[13] Becker H, Brach D, Otto A and Weber H-J 1991 *Rev. Sci. Instrum.* **62** 1196
[14] Jona F and Shirane G 1962 *Ferroelectric Crystals* (Oxford: Pergamon)
[15] Thomaz M T and Nussenzveig H M 1982 *Ann. Phys., NY* **139** 14
[16] Chandrasekhar S 1960 *Proc. R. Soc.* A **259** 531
[17] Weber H-J 1983 *Sov. Phys.–Crystallogr.* **28** 187
[18] Weber H-J 1979 *Z. Kristallogr.* **149** 269